

The ROSAT Deep Surveys

G. Hasinger¹, I. Lehmann¹, R. Giacconi², M. Schmidt³, and J. Trümper⁴ and G. Zamorani⁵

¹ Astrophysikalisches Institut Potsdam, An der Sternwarte 16, 14482 Potsdam, Germany

² European Southern Observatory, Garching, Germany

³ California Institute of Technology, Pasadena, USA

⁴ Max-Planck-Institut für extraterrestrische Physik, Garching, Germany

⁵ Osservatorio Astronomico, Bologna, Italy

Abstract. The ROSAT Deep Survey in the *Lockman Hole* is the most sensitive X-ray survey performed to date, encompassing an exposure time of 200 ksec with the PSPC and 1.2 Msec with the HRI. The source counts reach a density of $\sim 1000 \text{ deg}^{-2}$ at a limiting flux of $\sim 10^{-15} \text{ erg cm}^{-2} \text{ s}^{-1}$. At this level 70–80% of the 0.5–2 keV X-ray background is resolved into discrete sources. Because of the excellent HRI positions, 83 X-ray sources with fluxes (0.5–2 keV) above $1.2 \times 10^{-15} \text{ erg cm}^{-2} \text{ s}^{-1}$ could be optically identified so far utilizing deep optical CCD images, NIR photometry and Keck spectroscopy, only 11 sources above this flux limit remain unidentified. The majority of objects turned out to be active galactic nuclei (AGN) with minority contributions of clusters of galaxies, stars and some individual galaxies. These deep pencil beam data together with a number of shallower ROSAT surveys define the source counts over six orders of magnitude in flux and provide a unique tool of unprecedented quality to study the cosmological evolution of AGN, which can easily provide the bulk of the extragalactic X-ray background and could give an important contribution to the total background light in the universe.

1. Introduction

Deep X-ray surveys using ROSAT, ASCA and BeppoSAX have resolved a significant fraction of the cosmic X-ray background (XRB) into discrete sources (Hasinger et al. 1998a, hereafter paper I) and optical identifications (Schmidt et al. 1998, hereafter paper II) are demonstrating that the XRB is largely due to accretion onto massive black holes, integrated over cosmic time. The deep soft X-ray surveys have detected a larger surface density of AGN than in any other waveband and find significant evolution in the space density of high-luminosity AGN contrary to the pure luminosity evolution which was the standard assumption so far (Hasinger 1998). However, considerable uncertainties still exist for the evolution of low-luminosity AGN (Schmidt et al. 1999; Miyaji, Hasinger & Schmidt, 1999) and at redshifts above 3.

The characteristic hard spectrum of the XRB can only be explained if most AGN spectra are heavily absorbed (see e.g. Comastri et al. 1995). Thus as much as 80-90% of the light produced by accretion may be absorbed by gas and dust clouds, which according to recent models could reside in nuclear starburst regions that feed the AGN (Fabian et al. 1998). This scenario would have important consequences for the current attempts to understand black hole and galaxy formation and evolution: The absorbed AGN will suffer severe extinction and therefore, unlike classical QSOs, would not be prominent at optical wavelengths. If most of the accretion power is being absorbed by gas and dust, it will have to be reradiated in the FIR range and be redshifted into the sub-mm band. AGN could therefore contribute a substantial fraction to the recently discovered cosmic FIR/sub-mm background which has already partly been resolved by deep SCUBA surveys (Almaini et al. 1999). The AGN light therefore needs to be taken into account when studying the star formation history in the early universe.

In this review we give a progress report of our studies of the XRB with emphasis on the ROSAT ultradeep HRI survey (section 2) and its optical/NIR identification (section 3). Surveys at harder X-rays are presented in context with the population synthesis models in section 4 and the X-ray luminosity function of galaxies and AGN, its cosmological evolution, and the contribution of AGN to the history of star formation in the early universe are discussed in section 5. A Hubble constant of $H_0 = 50 \text{ km/s/Mpc}$ and a deceleration parameter $q_0 = 0.5$ are assumed throughout the paper.

2. The ROSAT Ultradeep HRI Survey

The ROSAT Deep Survey (RDS) project consists of pointed observations with the ROSAT PSPC and HRI detectors in the direction of the Lockman Hole (paper I) and in the Marano field (Zamorani et al. 1999). We have obtained a pencil beam survey in the Lockman Hole with the deepest X-ray observation ever performed. Images of 200 ksec observation time with the ROSAT PSPC (see Fig. 1) define the *Deep PSPC Survey* (Hasinger et al. 1993), and

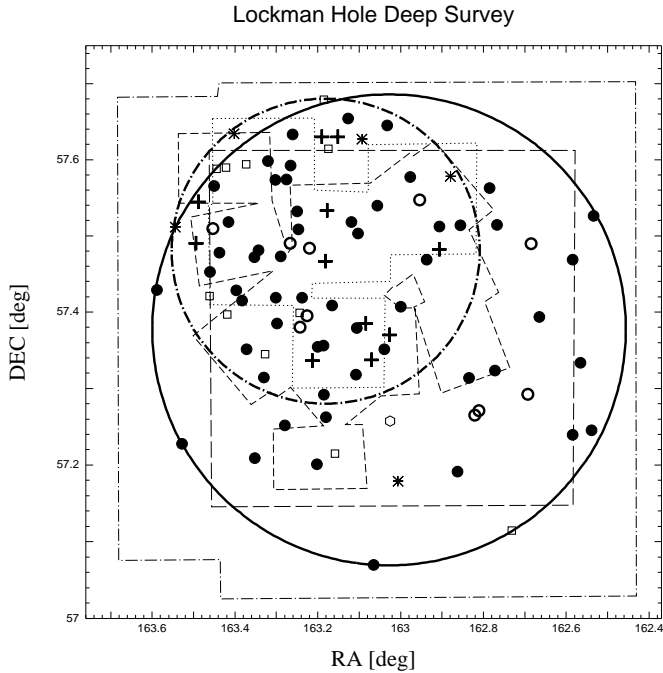


Fig. 1. Overview of X-ray surveys and optical/NIR coverage of the Lockman Hole. The thick solid circle gives the location of the PSPC deep survey with an 18.5 arcmin radius field. The thick dot-dashed circle shows the location of the HRI ultra-deep survey 12 arcmin radius field. The thin dashed line outlines the Keck R-band images available so far. Most of them have exposure times of 5 minutes, seeing 0.7" and limiting magnitudes about $R=25.5$ (see Lehmann et al. 1999). The thin dotted line outlines the Calar Alto K-band images available so far (courtesy T. Stanke, M. McCaughrean). Exposure times are around 40 min each giving a limiting magnitude in K' of about 19.7. The long-dashed square indicates the area covered by UH 8K-images (courtesy G. Luppino) in V and I; seeing is about 0.7-1 arcsec, limiting magnitude around 24. The thin dash-dotted line shows the area covered by CCD drift scans in V and I using the 4-shooter camera on the Palomar 200" telescope (courtesy J. Gunn and D. Schneider). The field has also been mosaicked with CCD exposures from the UH 88" in B and R (courtesy J. MacKenty and R. Burg). The symbols depict the location of the X-ray sources in our total sample. Filled circles are spectroscopically identified broad-line AGN (ID classes a-c; see paper II). Open circles are narrow-line AGN (ID classes d and e; paper II). The open hexagon is one galaxy. Open squares are clusters of galaxies. Asterisks are stars. Plus signs are the as yet unidentified sources.

exposures totalling 1.2 Msec in a smaller area (Fig. 1) are the basis for the *Ultra-deep HRI Survey* (paper I). The ultra-deep ROSAT HRI survey now reaches a surface density of ~ 1000 sources deg^{-2} at a flux of $10^{-15} \text{ erg cm}^{-2} \text{ s}^{-1}$ and 70–80% of the soft X-ray background has been resolved into discrete sources. The fluctuation analysis of the PSPC survey resolved about 85–100% (Hasinger et al. 1993).

The Lockman Hole is also target for other deep multifrequency surveys. In the optical band, a mosaique of UH 88" CCD images (B, R), Keck R-band CCD images, Palomar 5m drift scans (V, I) and UH 8K images (V, I) have been obtained, which form the basis of our spectroscopic follow-up identifications (paper II, see also Fig. 1). Deep VLA radio mosaic observations (deRuiter et al. 1997) and, recently, deep ASCA (Ogasaka et al. 1998) and BeppoSAX (Giommi 1999) hard X-ray images have been acquired in the 0.3 deg^2 survey region. The field will soon be surveyed by the Chandra X-ray Observatory (AXAF) and by XMM at hard X-rays in GT and PV-time, respectively. The Lockman Hole was also covered by a deep and medium-deep 7μ and 15μ mid-IR survey with ISO-CAM (Elbaz et al. 1998) and a 90μ far-IR survey with ISOPHOT (Kawara et al. 1998) and is targeted in ongoing SCUBA observations. Finally, the Lockman Hole is one of the CADIS fields (Thommes et al. 1998) and a deep K-band survey with the Omega-Prime camera at Calar Alto has been started (see Fig. 1).

3. Optical/NIR identifications

Optical counterparts of the weakest X-ray sources are very faint ($R > 24$) and require good, unconfused X-ray positions and high-quality optical spectra. For the Lockman Hole the optical follow-up spectroscopy could largely be done with long-slit and multi-slit spectroscopy at the Keck telescope. A catalogue of spectroscopic optical counterparts for a complete sample of 50 ROSAT PSPC sources in the Lockman Hole with 0.5–2 keV fluxes brighter than $1.1 \times 10^{-14} \text{ erg cm}^{-2} \text{ s}^{-1}$ in a solid angle of 0.299 deg^{-2} and fluxes brighter than $5.5 \times 10^{-15} \text{ erg cm}^{-2} \text{ s}^{-1}$ in a solid angle of 0.136 deg^{-2} has been published in paper II. The large majority ($> 80\%$) of the X-ray sources in the deep PSPC survey turned out to be AGN. Most of those are QSOs and Sy1 galaxies with at least one broad emission line in their optical spectra. A non-negligible fraction ($\sim 16\%$) shows only narrow emission lines in their spectra. We interpret these as type 2 AGN because of the presence of high excitation [NeV] emission lines and/or high X-ray luminosity ($L_X > 10^{43} \text{ erg s}^{-1}$). In the published catalogue of the 50 X-ray sources in the deep PSPC survey, there are four unidentified objects. In the meantime one of these four sources (#36) has been identified as an AGN at $z=1.52$ (Lehmann et al. 1999). The status of other unidentified sources are discussed in the following together with the sample of X-ray sources from the ultra-deep HRI survey with fluxes fainter than $5.5 \times 10^{-15} \text{ erg cm}^{-2} \text{ s}^{-1}$. Among the latter objects is the highest redshift X-ray selected QSO at $z=4.45$ (Schneider et al. 1998).

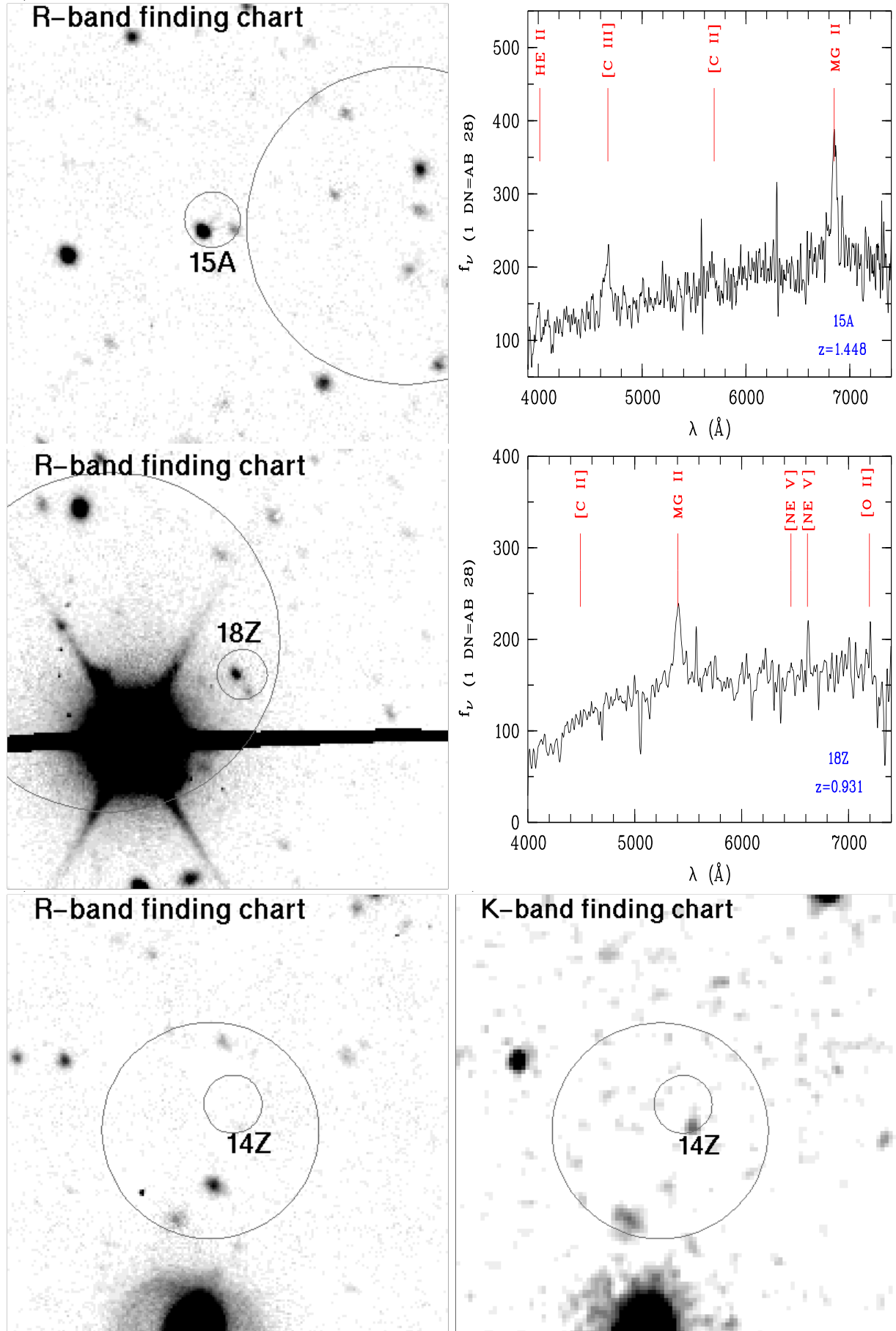


Fig. 2. Finding charts ($85'' \times 85''$) and optical spectra of selected X-ray sources in the ROSAT ultradeep HRI survey. The small circles and large error circles are from HRI and PSPC, respectively.

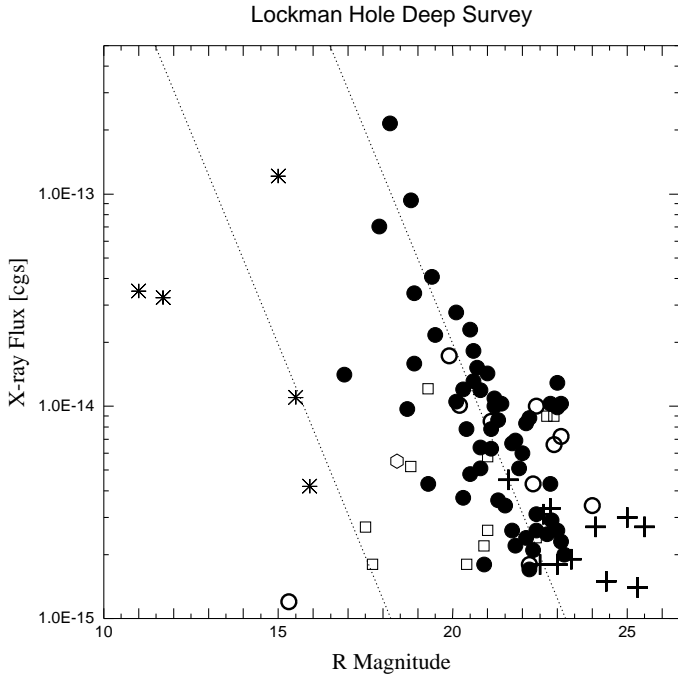


Fig. 3. Correlation between X-ray flux and optical R magnitude for all objects in the Lockman Hole survey. Symbols are the same as in figure 1. For the unidentified sources we show the brightest optical counterpart in the 90% error circle.

3.1. Sample selection

There are systematic differences between the deep PSPC and the ultra-deep HRI pointing in the Lockman Hole. The HRI pointing center is shifted with respect to the PSPC center by about 9 arcmin in North-East direction (paper I, see Fig. 1). The conversion between count rates observed in the PSPC hard band (PI channels 51-201) to 0.5–2 keV fluxes is straightforward because of the similar band-passes, while the HRI detector is sensitive in the 0.1–2 keV range leading to a substantial model-dependence in the count rate to flux conversion. Time variability of X-ray sources can also lead to different fluxes for the same source in different exposures (see e.g. paper II). In order to nevertheless construct a well defined, reliable set of faint X-ray sources combining both the PSPC and the HRI data we have used a sample definition different than that in paper I.

First we have selected all HRI sources with off-axis angle less than 12 arcmin from the HRI pointing center. Their 0.5–2 keV X-ray fluxes were determined from the HRI count rates and a renormalized count-to-flux conversion factor using all sources detected jointly in the HRI and the PSPC. Thus the epoch and fluxes of this part of the survey are defined by the HRI pointing. The approximate flux limit of the HRI survey is $1.2 \times 10^{-15} \text{ erg cm}^{-2} \text{ s}^{-1}$ (see paper I) and the solid angle 0.126 deg^{-2} . In addition, we use the deep PSPC sources which do not fall into the HRI sample and

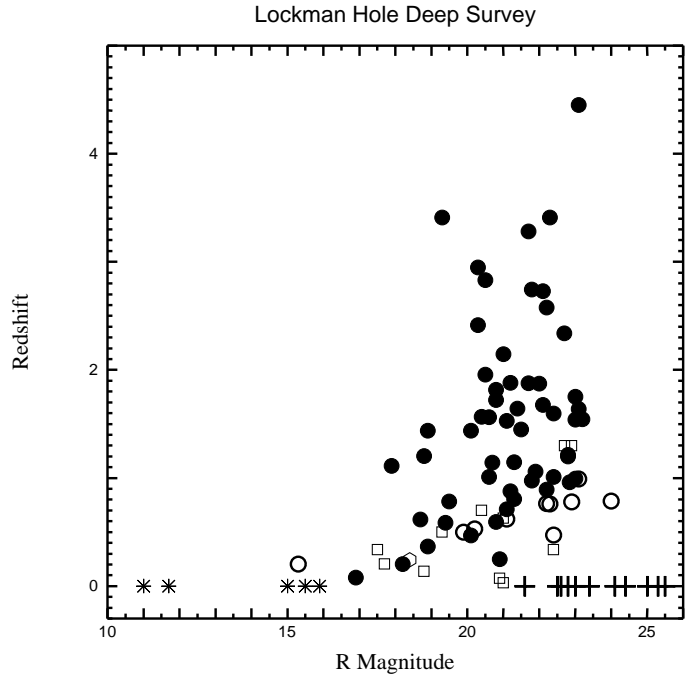


Fig. 4. Correlation between optical R magnitude and redshift for all objects in the Lockman Hole survey. Symbols as in Fig. 1. Unidentified sources (crosses) are shown at redshift zero.

have PSPC off-axis angles between 12.5 and 18.5 arcmin and PSPC fluxes larger than $9.6 \times 10^{-15} \text{ erg cm}^{-2} \text{ s}^{-1}$ (solid angle 0.071 deg^{-2}) or PSPC off-axis angles smaller than 12.5 arcmin and PSPC fluxes larger than $5.5 \times 10^{-15} \text{ erg cm}^{-2} \text{ s}^{-1}$ (solid angle 0.119 deg^{-2}). This latter part of the sample is statistically independent from the HRI sample and defined by the epoch of the PSPC observations. It is very similar to that part of the sample in papers I and II, which is not covered by the HRI pointing. The total number of sources in the sample is 94 (68 HRI and 26 PSPC). The new sample definition results in some changes compared to the catalogue of the 50 brightest sources presented in paper I and II. A few sources are lost completely (e.g. the previously unidentified source #116), others have a higher flux because of time variability.

The importance of an excellent X-ray position accuracy in order to avoid confusion and to obtain unique identifications of extremely faint sources has been emphasized in paper I and II. Figure 2 shows three examples of optical finding charts, based on deep Keck R-band exposures, where the very good HRI positions (90% error radius 2–5 arcsec) pointed out unique optical counterparts which would have been very hard to identify from the PSPC positions alone. The first example (#15) is a case where a $z=1.45$ QSO, pinpointed uniquely by the HRI, lies outside the relatively large PSPC 90%-error circle. The second source (#18) was originally misidentified with the bright star in the PSPC error circle, until the HRI pointed out

a $z=0.93$ QSO only a few arcsec from the star. The third case is ROSAT #14 where no optical counterpart is found in the HRI error circle to $R < 24.5$. A 45min K' -band exposure with the OMEGA-Prime camera on the Calar Alto 3.5m telescope was obtained in December 1997. Interestingly, the X-ray error circle contains a $K'=19.5$ infrared counterpart associated with an $R=25$ optical object and a very red colour of $R - K' = 5.5$. We do not yet have a spectroscopic identification of this object, but assume that it is a high-redshift and/or obscured AGN.

In the Lockman Hole Deep survey most optical counterparts have magnitudes in the range $R=18-25.5$. With the excellent HRI positions typically only one or two counterparts are within the X-ray error circle. In Fig. 3 the X-ray fluxes of our sources are plotted against the magnitude of their optical counterparts or, in case of no identification, of the brightest optical candidate in the error box. The objects with spectroscopic identifications are marked with different symbols, while the unidentified sources are shown with crosses. As shown in this figure, we have a 100% complete identification for 53 sources with fluxes above $5 \times 10^{-15} \text{ erg cm}^{-2} \text{ s}^{-1}$ in this sample, while at fainter fluxes 11 out of 41 sources remain unidentified. The large majority of optical identifications even at these faint fluxes are broad-line AGN (filled circles) with X-ray/optical flux ratios typically scattering around unity (right dotted line). This is in marked contrast to the findings of McHardy et al. (1998), who in their deep PSPC survey claim to find a majority of galaxies (or narrow-line AGN) which have similar X-ray fluxes but on average lower f_X/f_{opt} ratios. This indicates a substantial fraction of misidentifications in the latter study.

Figure 4 shows a correlation between optical magnitude and redshift for all X-ray sources. For the purpose of deriving luminosity functions, it is important to note, that about 20% of our AGN have $z > 2$ and about 40% $z > 1.5$. Clusters of galaxies and narrow-line AGN are typically found at redshifts below 1.

3.2. NIR photometry

Optical spectroscopy from Keck becomes exceedingly time consuming for objects with $R > 23.5$, which is roughly our current spectroscopic limit. A few of the unidentified sources in Fig. 3 are brighter than this limit. For some of those we just were not able to take spectra yet and some show noisy spectra without obvious features. Five unidentified sources have very faint optical counterparts ($R > 23.5$). For these objects we were able to obtain NIR images down to $K' \sim 19-20$. Because of the large field of view of Omega-Prime (42 arcmin^2), these images cover almost half of the ultra-deep HRI survey field. We are therefore able to derive $R-K'$ colours for almost half of our sample. Figure 5 shows a colour-magnitude diagram for all objects detected in the K' -images, including the X-ray sources in the K -band survey. This figure clearly

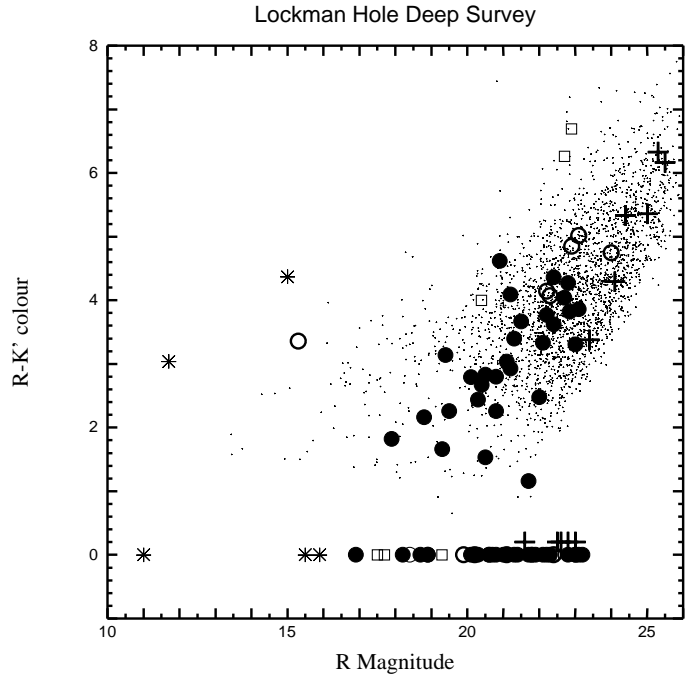


Fig. 5. Colour-magnitude diagram between R magnitude and $R - K'$ colour for objects in the Lockman Hole survey. Small dots are all sources detected in the Lockman Hole K -band survey. Symbols of X-ray sources as in Fig. 1. Those X-ray sources not covered by the K survey are plotted at $R - K' = 0$ or 0.2 . The optically faintest unidentified sources have red $R - K'$ colours, only exceeded by galaxies associated with a high-redshift cluster (see below).

shows, that all X-ray counterparts with optical magnitudes fainter than $R=23.5$ have red colours ($R - K' > 4$). The identified X-ray sources with such red colours are either clusters of galaxies at redshifts above 1 (see below) or low-luminosity, absorbed AGN at various redshifts. We can therefore safely assume that the faint unidentified sources are part of the same population as the identified sources. A similar group of red X-ray sources has been found by Newsam et al. (1997).

3.3. Clusters of galaxies

The second most abundant class of faint X-ray sources in our sample are clusters and groups of galaxies (open squares in Fig. 3). Their surface density in our survey is $63 \pm 22 \text{ rmd} \text{ deg}^{-2}$, consistent with an extrapolation of the no-evolution $\log(N)-\log(S)$ found in the ROSAT Deep Cluster Survey by Rosati (1998) and their redshifts are typically below 0.7. A substantial fraction of the clusters and groups appear extended in the ultra-deep HRI image (see paper II).

The brightest extended X-ray source in the Lockman Hole (RX J105343+5735) shows a peculiar elongated double-lobed structure (see Fig. 6). The angular size of the X-ray source is $1.7 \times 0.7 \text{ arcmin}^2$, its X-ray flux

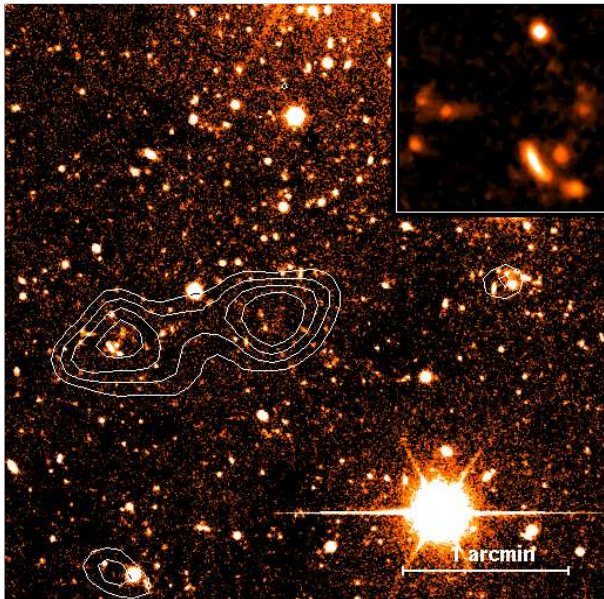


Fig. 6. ROSAT ultradeep HRI pointing X-ray contours of a region about $3 \times 3 \text{ arcmin}^2$ in the Lockman Hole, superposed on a 5 min Keck R band exposure. North is up and East is to the left. Three distinct X-ray sources are detected in this image: the extended source RX J105343+5735 with its eastern and western lobe, a cluster of galaxies at $z=0.7$ to the West and a QSO at $z=2.572$ to the South. The insert in the upper right is a $20 \times 20 \text{ arcsec}^2$ zoomed cutout of the image close to the center of the eastern lobe. A gravitationally lensed arc at a redshift of 2.570 is detected there.

$2 \times 10^{-14} \text{ erg cm}^{-2} \text{ s}^{-1}$. R-band optical imaging from the Keck telescope revealed only a marginal excess of galaxies brighter than $R=24.5$. The brightest galaxy close to the center of the eastern emission peak turned out to be a gravitationally lensed arc at $z=2.570$ (see Fig. 7), suggesting that the X-ray emitting object is most likely a cluster of galaxies. This is the first detection of a gravitational arc which is optically brighter than any of the components of the lens. X-ray and optical data on this cluster have been published in a recent paper (Hasinger et al. 1998b), where it was argued that RX J105343+5735 is a moderately luminous cluster at a redshift around unity, based on a comparison of lensing surface mass density, X-ray luminosity, morphology and galaxy magnitudes with a large sample of clusters of known distance. In the meantime, the cluster was covered by one of the K-band images (see above), which clearly shows relatively bright, very red ($R - K' > 6$) cluster galaxies at the X-ray centroids of the two lobes (see also fig 5). A very high redshift (~ 1.3) is thus expected for this object.

4. Hard X-ray surveys

The X-ray background has a significantly harder spectrum than that of the sources resolved in the soft band. This led to the assumption that a large fraction of the

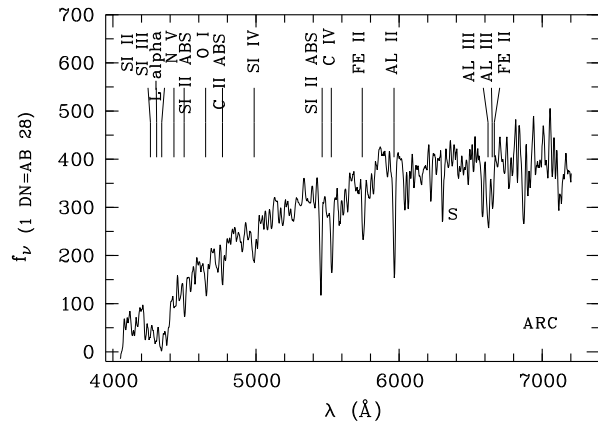


Fig. 7. Keck LRIS spectrum of the arc in RX J105343+5735. The wavelengths of prominent UV metal absorption lines, redshifted to $z=2.570$ are indicated. “S” denotes the position of a strong sky line. The spectrum is typical for a high-redshift star-forming galaxy.

background flux is due to obscured AGN, as originally proposed by Setti and Woltjer (1989). Models following the unified AGN schemes, assuming an appropriate mixture of absorbed and unabsorbed AGN spectra folded with cosmological AGN evolution models, can quite successfully explain the shape of the background spectrum over the whole X-ray band as well as a number of other observational constraints (e.g. Comastri et al. 1995). The distribution of absorption column densities among different types of AGN is one of the major uncertainties in this kind of modelling (see below). Observationally, it has so far only been possible to derive this for local Seyfert galaxies selected at hard X-rays (see e.g. Schartel et al. 1997) or from optical emission lines (Maiolino et al. 1999). The standard X-ray background population synthesis models (Matt & Fabian 1994; Madau et al. 1994; Comastri et al. 1995) assume that the absorption distribution is independent of X-ray luminosity and redshift.

An immediate consequence of these types of models is that the radiation produced by accretion processes in AGN emerges completely unabsorbed only at energies well above 10 keV, thus producing the observed maximum of the XRB energy density at $\sim 30 \text{ keV}$. Comparison between the background energy density at 30 keV and at 1 keV leads to the suggestion that most (80–90%) of the accretion power in the universe might be absorbed, implying a very large solid angle of the obscuring material as seen from the central source. Fabian et al. (1998) suggest that circumnuclear starburst regions are responsible for the large covering factor. They may be both triggering and obscuring most of the nuclear activity. Recently Fabian and Iwasawa (1999) have shown that these AGN background synthesis models can explain the mass distribution of dark remnant black holes in the centers of nearby galaxies by conventional accretion which is largely hidden by obscuration.

The existing background synthesis models predict that a large part of the hard X-ray background comes from significantly absorbed objects, which are almost absent in the soft band, even at the faintest ROSAT limit. As a consequence, a significant test for these models would be the comparison of their predictions with the results of optical identifications of a complete sample of sources selected at faint fluxes in the hard X-ray band.

Because of the technological challenge for X-ray imaging above 2 keV, hard X-ray surveys are just becoming available now. A large sky survey (LSS) with a limiting flux of 10^{-13} erg cm $^{-2}$ s $^{-1}$ (2–10 keV) near the North Galactic Pole was performed with the ASCA satellite (Ueda et al. 1998). Recently, ASCA data have been used by Cagnoni et al. (1998) to derive the 2–10 keV log(N)–log(S) down to fluxes slightly below 10^{-13} erg cm $^{-2}$ s $^{-1}$. The deepest ASCA surveys (Georgantopoulos et al. 1997; Ogasaka et al. 1998) resolve source counts down to 2–10 keV fluxes of 5×10^{-14} erg cm $^{-2}$ s $^{-1}$. At surface densities of typically 100 sources deg $^{-2}$ these surveys are heavily confused due to ASCA’s limited angular resolution. An analysis of the spatial fluctuations in deep ASCA images (Gendreau et al. 1997) probes the 2–10 keV X-ray source counts down to a flux limit of 2×10^{-14} erg cm $^{-2}$ s $^{-1}$, resolving about 35% of the extragalactic 2–10 keV X-ray background.

A new High Energy Large Area Survey (HELLAS) has been started with BeppoSAX in the 5–10 keV band, which is particularly well suited for this instrument because of the relatively large throughput at high energies and a significantly sharper point spread function compared with ASCA. A surface density of ~ 20 sources deg $^{-2}$ is reported (Fiore et al. 1998) at a 5–10 keV flux limit of 5×10^{-14} erg cm $^{-2}$ s $^{-1}$, indicating that 30–40% of the background in this energy band has already been resolved.

The hard X-ray log(N)–log(S) data so far are in good agreement with the predictions of the population synthesis models (Comastri et al. 1999; Miyaji, Hasinger & Schmidt 1999). Following these models, a large fraction of X-ray sources at faint fluxes should be substantially absorbed and therefore their counterparts are expected to have optical spectra typical of Seyfert 2 galaxies. Programs to optically identify the sources from these hard surveys have already started and indeed find typically AGN counterparts (Boyle et al. 1998; Akiyama et al. 1998; Fiore et al. 1999), but the large positional uncertainty together with the relatively faint optical counterparts slows down progress so that sample sizes are still small.

Deep hard surveys with ASCA and BeppoSAX have also been taken in the Lockman Hole, where due to the existence of the ROSAT HRI data a cross-identification between the soft and hard X-ray data is readily available. Details of the ASCA and BeppoSAX surveys will be presented elsewhere (Ishisaki et al. 1998; Giommi 1999). A somewhat surprising result is that almost all hard X-ray sources in the ASCA and BeppoSAX images of the

Lockman Hole have relatively bright soft X-ray counterparts. This appears to be inconsistent with the simple XRB population synthesis models, which would predict a substantial fraction of hard sources not detectable in the soft band. We may see here effects that have been neglected in the population synthesis models, like e.g. partial obscuration or unabsorbed soft spectral components in heavily obscured AGN. Another possible effect would be a dependence of the obscuration distribution on luminosity and/or redshift. Despite occasional discoveries of absorbed (type 1.5-2) QSOs (Almaini et al. 1995; Ohta et al. 1997; Zamorani et al. 1999), there is observational evidence that high luminosity and/or high redshift AGN are on the average much less absorbed than local Seyfert galaxies (see e.g. Fig. 4; Halpern et al. 1998; Miyaji, Hasinger & Schmidt, 1999).

Detailed information about the absorption distribution of the AGN population as a function of luminosity and redshift is a necessary ingredient to derive the AGN X-ray luminosity function (XLF) and its cosmological evolution, which in turn is input into the population synthesis models for the X-ray background. So far, the derivations of the AGN XLF have largely ignored the effects of X-ray absorption (see below). First global, simultaneous fits of the XLF, X-ray background spectrum and absorption distribution have just been performed (Schmidt et al. 1999; Miyaji, Hasinger & Schmidt, 1999a), but are still quite uncertain because of the large number of parameters and the possible hidden correlations involved. Upcoming deep surveys with the Chandra observatory (AXAF) and XMM with very high sensitivity and good positional accuracy in the hard band together with optical identifications from the VLT and the Keck telescopes are expected to yield a solid statistical basis to disentangle these various effects and lead to a new, unambiguous population synthesis for the X-ray background.

5. AGN cosmological evolution

As discussed above, information about the cosmological evolution of the AGN population is a crucial input into the background synthesis models, but it can not be obtained without taking into account the AGN absorption distribution. However, the AGN X-ray luminosity function in the 0.5–2 keV band has so far mainly been derived ignoring the effects of absorption. First attempts to study AGN cosmological evolution from the Einstein Medium Sensitivity Survey (EMSS; Della Ceca et al. 1992) or from a combination of medium deep ROSAT fields with the EMSS (Boyle et al. 1994) determined the local AGN XLF which has the shape of a broken power law. Their data are consistent with pure luminosity evolution proportional to $(1+z)^{2.7}$ up to a redshift $z_{max} \approx 1.5$, similar to what was found previously in the optical range. This result has been confirmed and improved by more extensive or deeper studies of the AGN XLF, e.g. the RIXOS project (Page et al.

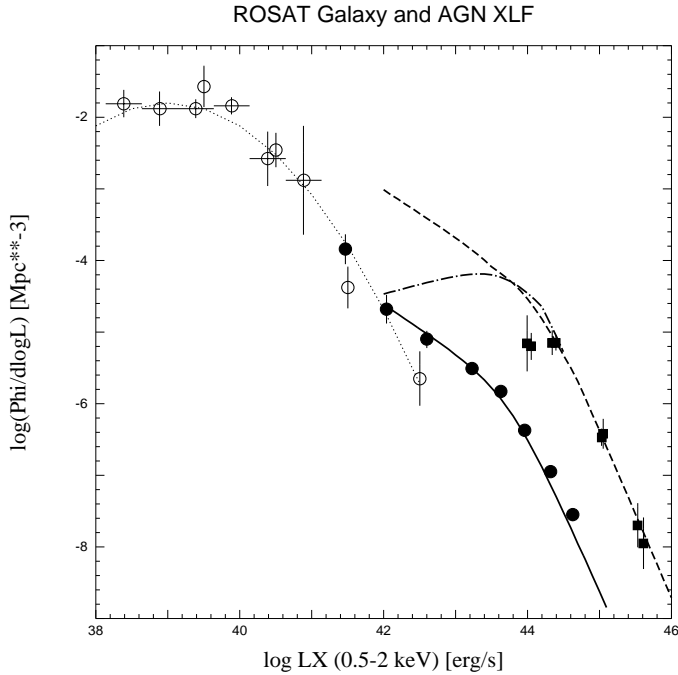


Fig. 8. X-ray (0.5–2 keV) Luminosity functions for AGN and galaxies from ROSAT surveys. The local galaxy luminosity function (open circles and dotted line) has been derived by Hasinger (1998) from the ROSAT Bright Survey (Fischer et al. 1998; Schwöpe et al. 1999) and from a volume-limited sample of local galaxies (Schmidt et al. 1996). The AGN luminosity function (filled circles, from Miyaji et al. 1999b) is shown only for nearby objects ($z < 0.2$) and very distant objects ($z > 1.6$). Two different luminosity-dependent density evolution models have been fit to the data, one which is close to a pure density evolution model (LDDE2, Miyaji et al. 1999b; dashed line) and one where evolution slows down substantially for low luminosities (LDDE1, Miyaji, Hasinger & Schmidt, 1998; dash-dotted line). Both models are consistent with all available constraints; their predictions for the density of low luminosity AGN, however, diverge by more than one order of magnitude.

1996) or the UK deep survey project (Jones et al. 1997). However, these studies were hampered by the uncertain crosscalibration between Einstein and ROSAT.

In the meantime optical identifications of a large number of ROSAT X-ray surveys at various flux limits and solid angle coverage have been completed, so that a new AGN soft X-ray luminosity function could be determined, based on ROSAT surveys alone (Hasinger 1998; Miyaji, Hasinger & Schmidt, 1998+1999b; Schmidt et al. 1999). The $\log(N)$ – $\log(S)$ function of the overall sample covers six orders of magnitude in flux and agrees within $\sim 10\%$ in the overlapping flux regions between different surveys (Hasinger 1998).

Contrary to the previous findings, the new XLF is not consistent with pure luminosity evolution. For the first time we see evidence for strong cosmological evolution of the space density of low-luminosity AGN (e.g. Seyfert

galaxy) XLF out to a redshift 1–2, incompatible with pure luminosity evolution. Pure density evolution proportional to $\sim (1+z)^5$ provided a reasonable fit to the ROSAT data (Hasinger 1998), but overpredicts the total X-ray background, when extrapolated to lower luminosities. Therefore more complicated evolution models have to be taken into account. The latest treatments (Schmidt et al. 1999; Miyaji, Hasinger & Schmidt, 1998+1999b) agree that luminosity-dependent density evolution (LDDE) models, where the rate of density evolution is a function of luminosity, can match all constraints. This evolutionary behaviour is similar to the most recently determined optical QSO evolution (Wisotzki 1998).

Figure 8 compares the luminosity function for local and high-redshift AGN to the luminosity function of local normal and star bursting galaxies. The low-redshift AGN XLF connects smoothly to the galaxy XLF at X-ray luminosities of $L_X \approx 10^{42}$ erg s $^{-1}$. Around this luminosity there is some ambiguity about the relative contribution between the nuclear AGN light and diffuse galactic X-ray emission processes (see Lehmann et al. 1998). For clarity, measurements of the high-redshift AGN XLF are only shown for the two highest redshift shells ($1.6 < z < 2.3$ and $2.3 < z < 4.5$) from the data of Miyaji, Hasinger & Schmidt (1998). The apparent deficiency in the lowest luminosity bins is most likely due to incompleteness. Two luminosity-dependent density evolution models are shown, which fit all observational constraints well: the LDDE1 model from Miyaji, Hasinger & Schmidt (1999) (dash-dotted line), which is similar to the LDDE model of Schmidt et al. (1999) has a rapid slow-down of the density evolution below X-ray luminosities of 10^{44} erg s $^{-1}$ and produces $\sim 60\%$ of the extragalactic 0.5–2 keV background. The LDDE2 model (Miyaji et al. 1999) is not very much different from a pure density evolution model and produces $\sim 90\%$ of the soft background. The constraints for the XLF of faint, high-redshift Seyfert galaxies, which can produce a significant fraction of the soft X-ray background and, depending on absorption properties, an even larger fraction of the hard X-ray background, are therefore still quite uncertain (the range is a factor of ~ 25 at $\log L_X = 42$). The LDDE2 model predicts a high-redshift AGN space density which is close to that of local normal galaxies just above the break of the luminosity function and to that of high-redshift galaxies. On the contrary, the LDDE1 model predicts a dearth of high-redshift Seyfert galaxies. A choice between these two possibilities will soon be possible with the even deeper X-ray surveys to be performed with the Chandra and XMM observatories.

5.1. The space density of high-redshift QSO

The X-ray data can also give important new information on the AGN evolution at very high redshifts and therefore on the epoch of black hole formation and the accretion history in the early universe. It is well known from opti-

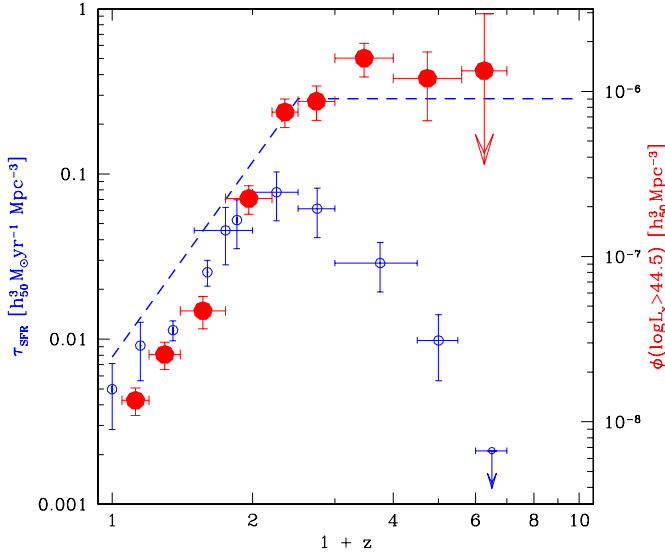


Fig. 9. Cosmic star formation history τ_{SFR} (left Y-axis) compared to the space density ϕ of luminous X-ray selected QSOs (right Y-axis). Filled circles give the comoving number density of ROSAT QSOs with $\log L_X > 44.5 \text{ erg s}^{-1}$ (from Miyaji et al. 1998). Open circles give the optical/UV measurements of the star formation rate compiled by Blain et al. 1998. The dashed line indicates the simplest star formation history model by Blain et al., which explains the whole FIR/sub-mm background light by dusty star formation. Note the similarity between this model and the QSO space density.

cal samples that the strong evolution of the space density of high luminosity QSOs slows down beyond a redshift of ~ 1.5 and that the space density decreases significantly beyond $z \approx 2.7$ (see e.g. Schmidt, Schneider & Gunn 1995). Different selection techniques have to be used below and above a redshift of ~ 2.2 leading to possible systematic uncertainties in the optical data. Radio-selected QSOs, however, confirm the decline at high redshift and indicate that it is apparently not due to an increase in dust obscuration (Shaver et al. 1998). The ROSAT sample of QSOs allows now for the first time to determine the space density of X-ray selected AGN in the whole range of $0 < z < 5$ with one technique. Figure 9 (right scale) shows the space density of AGN with X-ray luminosity $\log L_X > 44.5 \text{ erg s}^{-1}$ as a function of redshift. Above this luminosity the XLF is a steep power law for all observed redshift shells and the data in Fig. 9 have been determined by assuming the slope to be independent of redshift and fitting the normalization of the XLF (Miyaji, Hasinger & Schmidt, 1998). The X-ray data do not show a significant decrease of the space density of high-redshift, high-luminosity X-ray selected AGN and appear to be marginally inconsistent with the optical and radio determinations (Miyaji, Hasinger & Schmidt, 1998). However, the X-ray surveys still suffer from small sample sizes at high redshift (see Fig. 4), so that significantly larger solid angles have to be covered to a similar depth and optical completeness as the ultra-deep

HRI survey i in order to get a clear picture of the AGN density at high redshift. The array of planned Chandra and XMM surveys in other fields than the Lockman Hole will be of great help in this respect.

5.2. AGN contribution to the star formation history

The star formation history in the universe out to redshifts of four has been studied in the last few years by optical and NIR observations using ground-based telescopes and deep photometric surveys with the Hubble Space Telescope (see e.g. Blain et al., 1998, for a recent review). The open circles in Fig. 9 show the compilation of the most recent observational determinations of the optical/UV star forming rate (SFR) by Blain et al. (left scale), which suggest that star formation peaked at a redshift around 1–2. These data points, however, have to be regarded as lower limits of the true SFR because much of the light emitted in star bursts can be significantly obscured. Recently the far-infrared/sub-mm extragalactic background light (FIB), the equivalent of the X-ray background at very long wavelengths, has been discovered (Puget et al. 1996; Fixsen et al. 1998). Deep SCUBA surveys have detected a population of optically faint galaxies, luminous in the sub-mm band, which could produce a significant fraction of the FIB signal (Smail, Ivison & Blain 1997; Hughes et al. 1998; Barger et al. 1998). Source counts of dusty galaxies and AGN in the sub-mm band are strongly weighted towards high redshift because of the large negative K-correction of the very steep dust spectra (Blain & Longair 1993). If all of the FIB should be due to star forming processes, a large population of strongly obscured star bursting galaxies would be missing from the optical/UV surveys at high redshifts. The dashed line in figure 9 sketches one of the SFR models by Blain et al., that is able to produce all of the FIB by early star formation. These models still have some drawbacks, however, because this massive early star formation would likely overproduce the heavy elements and consume a large fraction of all baryons in the universe into stars (Blain et al. 1998).

It is interesting to note that the star formation rate required to produce the FIB light has a cosmic history which is very similar to the dependence of the AGN space density on redshift (see Fig. 9). Could it be, that active galactic nuclei contribute significantly to the faint sub-mm source population? The X-ray background population synthesis models have recently been used by Almaini et al. (1999) to predict the AGN contribution to the sub-mm background and source counts. Depending on the assumptions about cosmology and in particular on the AGN space density at high redshifts (see above) they predict that between 20 and 100% of the sub-mm source counts at the current SCUBA flux limit could be associated with active galactic nuclei. Interestingly, the first optical identifications of SCUBA sources already indicate a substantial contribution from AGN (Cowie 1999).

Another, largely independent line of arguments leads to the conclusion that accretion processes may produce an important contribution to the extragalactic background light. Dynamical studies (e.g. Magorrian et al. 1998) come to the conclusion that massive dark objects, most likely dormant black holes, are ubiquitous in nearby galaxies. There is a correlation between the black hole mass and the bulge mass of a galaxy: $M_{BH} \approx 6 \times 10^{-3} M_{Bulge}$. Since gravitational energy release through standard accretion of matter onto a black hole is producing radiation about 100 times more efficiently than the thermonuclear fusion processes in stars, the total amount of light produced by accretion in the universe should be of the same order of magnitude as that produced by stars. A more detailed treatment following this argument comes to the conclusion that the AGN contribution should be about 1/5 of the stellar light in the universe (Fabian & Iwasawa, 1999).

Regardless of whether the FIR light of AGN is from dust heated by stellar processes or by accretion onto the massive black hole, these studies indicate that a large contribution to the light emission history in the early universe could come from sources associated with AGN, which are most easily pin-pointed by sensitive X-ray observations. Future joint sub-mm/X-ray deep surveys will therefore be a very powerful tool to disentangle the different processes dominating the universe in the redshift range $2 < z < 5$.

Acknowledgements. The ROSAT project is supported by the Bundesministerium für Forschung und Technologie (BMFT), by the National Aeronautics and Space Administration (NASA), and the Science and Engineering Research Council (SERC). This work has been supported in part by the DLR (former DARA GmbH) under grant 50 OR 9403 5 (G.H and I.L.) and by NASA grants NAG5-1531 (M.S.), NAG8-794, NAG5-1649, and NAGW-2508 (R.G.). G.Z. acknowledges partial support by the Italian Space Agency (ASI) under contract ARS-96-70.

References

- Almaini O. et al., 1995, MNRAS 277, L31
 Almaini O., Lawrence A., Boyle B., MNRAS (submitted)
 Akiyama M. et al., 1998, First XMM workshop (astro-ph/9811012)
 Barger A.J. et al., 1998, Nat 394, 248
 Blain A.W. & Longair M.S., 1993, MNRAS 264, 509
 Blain A.W. et al., 1998, MNRAS (in press, astro-ph/9806062)
 Boyle B.J. et al., 1994, MNRAS 260, 49
 Boyle B.J. et al., 1998, MNRAS 296, 1
 Cagnoni I., Della Ceca R. and Maccacaro T. 1998, ApJ 493, 54
 Comastri A., Setti G., Zamorani G. and Hasinger G. 1995, A&A, 296, 1
 Comastri A. et al., 1999, Adv. Space Res., (in press)
 Cowie L., 1999, Proceeding of the 5th Maryland Conference: After the dark ages ...
 Della Ceca R. et al., 1992, ApJ 389, 491
 Elbaz D., Aussel H., Baker A.C., 1998, Proceedings of the NGST workshop, June, 98, p. 47 (astro-ph/9807209)
 Fabian A.C. et al., 1998, MNRAS 297, L11
 Fabian A.C., Iwasawa K., 1999, MNRAS (in press)
 Fiore F. et al., 1999, First XMM workshop, astro-ph/9811149
 Fischer J.U. et al., 1998, AN 319, 347
 Fixsen D.J. et al., 1998, ApJ (in press, astro-ph/9803021)
 Gendreau K.C., Barcons X. and Fabian A.C., 1998, MNRAS 297, 41
 Georgantopoulos I. et al., 1997, MNRAS 291, 203
 Giommi P. 1999, proceedings of Taormina workshop, (in press)
 Halpern J., Eracleous M., Forster K., 1998, ApJ 501, 103
 Hasinger G. et al., 1993, A&A 275, 1
 Hasinger G. et al., 1997, AN 318, 329
 Hasinger G., 1998, AN 319, 37
 Hasinger G. et al., 1998a, A&A, 329, 482 (paper I)
 Hasinger G. et al., 1998b, A&A, 340, L27
 Hughes D.H. et al., 1998, Nat 394, 241
 Ishisaki Y. et al., 1999, (in prep.)
 Jones L.R. et al., 1997, MNRAS 285, 547
 Kawara K. et al., 1998, A&A 336, L9
 Lehmann I. et al., 1998, this volume (astro-ph/9810214)
 Lehmann I. et al., 1999, A&A (in prep.)
 Madau P. et al., 1994, MNRAS 283 1388
 Magorrian J. et al., 1998, AJ 115, 2285
 Maiolino R. et al., 1999, Adv. Space Res. (in press)
 Matt G. & Fabian A.C., 1994, MNRAS 267 187
 McHardy I. et al., 1998, MNRAS 295, 641
 Miyaji T., Hasinger G., Schmidt M., 1998, this volume (astro-ph/9809398)
 Miyaji T. et al., 1999a, Adv. Space Res. (in press)
 Miyaji T. et al., 1999b, A&A (in prep.)
 Newsam A.M. et al. 1997, MNRAS 292, 378
 Ogasaka Y. et al. 1998, AN 319, 43
 Ohta K. et al., 1996, ApJ 458, L57
 Page M.J. et al., 1996, MNRAS 281, 579
 Puget J.-L. et al., 1996, A&A 308, L5
 Rosati P., 1998, AN 319, 79
 Rosati P. et al., 1998, ApJ 492, L21
 de Ruiter H. et al., 1997, A&A 319, 7
 Setti G. and Woltjer L. 1989, A&A 224, L21
 Schmidt K.-H., Boller T., Voges W., MPE report 263, 395
 Scharrel N. et al. 1997, A&A, 320, 696
 Schmidt M., Schneider D.P., Gunn J.E., 1995, AJ 110 68
 Schmidt M. et al. 1998, A&A, 329, 495 (paper II)
 Schmidt M. et al. 1999, this volume
 Schneider D. et al., 1998, AJ 115, 1230
 Schwobe A. et al., 1999, A&A in prep.
 Shaver P.A. et al., 1998 (astro-ph/9801211)
 Smail I., Ivison R.J., Blain A.W., 1997, ApJ 490, L5
 Thommes E. et al., 1998, MNRAS 293, L6
 Ueda Y. et al., 1998, Nature 391, 866
 Wisotzki L., 1998, AN 319, 257
 Zamorani G. et al., 1998, A&A (submitted)